Received: 8 September 2022 | Revised: 21 November 2022 | Accepted: 6 December 2022

DOI: 10.1002/bio.4422

RESEARCH ARTICLE

LUMINESCENCE The Journal of Biological and Chemical Luminescence WILEY

Optical, emission, and excitation dynamics of Eu^{3+}-doped bismuth-based phosphate glass for visible display laser applications

P. Reddi Babu[1] | Devarajulu Gelija[2] | Kedhareswara Sairam Pasupuleti[3] | B. Kiran Kumar[4] | N. John Sushma[5] | Moon-Deock Kim[2,3] | B. Deva Prasad Raju[1]

[1]Department of Physics, Sri Venkateswara University, Tirupati, India

[2]Institute of Quantum Systems (IQS), Chungnam National University, 99Daehak-ro, Daejeon, Yuseong-gu, Republic of Korea

[3]Department of Physics, Chungnam National University, 99Daehak-ro, Daejeon, Yuseong-gu, Republic of Korea

[4]Department of Physics, Government Degree College, Rayachoty, Andhra Pradesh, India

[5]Department of Biotechnology, Sri Padmavati Mahila Visvavidyalayam, Tirupati, India

Correspondence
B. Deva Prasad Raju, Department of Physics, Sri Venkateswara University, Tirupati-517 502, India.
Email: drdevaprasadraju@gmail.com

Moon-Deock Kim, Department of Physics, Chungnam National University, 99Daehak-ro, Yuseong-gu, Daejeon 34134, Republic of Korea.
Email: mdkim@cnu.ac.kr

Abstract

Eu^{3+}-doped-bismuth-based phosphate glasses with chemical equation $(60 - x)P_2O_5$–$20Bi_2O_3$–$10Na_2CO_3$–$10SrF_2$–xEu_2O_3 (PBNSEu), (where $x = 0$, 0.1, 0.5, 1.0, 1.5 and 2 mol%) were fabricated using the melt-quenching method. Obtain X-ray diffraction (XRD), energy-dispersive X-ray (EDAX), and Fourier transform infrared (FTIR) spectra were used to characterize the structure of the prepared PBNSEu glass. The J–O (Judd–Ofelt) intensity parameters (Ω_2, Ω_4) were estimated using photoluminescence emission spectra. When excited with a xenon lamp at $\lambda_{exc} = 394$ nm, the most intense red-emission transition occurred at ~612 nm ($^5D_0 \rightarrow {}^7F_2$). J–O intensity parameters were used to calculate radiative properties, whereas the radiative branching ratio (β_R), radiative transition probability (A_R), radiative lifetime (τ_R), and total radiative transition rate (A_t) were calculated for the transitions $^5D_0 \rightarrow {}^7F_J$ (where J = 0–4) and were obtained in the emission spectra for europium ion-doped in the current glass. Using the CIE1931 chromaticity coordinates axes, the colours of various concentrations of Eu^{3+} ion-doped PBNS glass were evaluated using the emission spectra. Temperature-dependent luminescence spectra were recorded for the optimized PBNSEu20 glass to calculate the activation energy. These results strongly suggested red components in w-LEDs and visible display laser applications.

KEYWORDS
Eu^{3+} ions, J–O parameters, phosphate glass, photoluminescence, radiative parameters, visible lasers

1 | INTRODUCTION

The unique properties of trivalent rare-earth (RE^{3+}) ions are expected to play an important role in current cutting-edge optical technology and, as a result, future advances. As active constituents in many new materials, these ions are vital to modern optical technology.[1–4] Chemical composition is a significant determinant of the optical properties associated with these materials, and establishes the nature and structure of the glass host matrix.[5] Recent attempts have concentrated on the crystal-field effects of host materials, local environments, and low phonon energies that minimize the multiphonon nonradiative relaxation of the RE^{3+} ion and thereby enhance the fluorescence levels of the RE^{3+} ions in the emission cross-section. Phosphate glass have garnered much scientific attention in recent years because of their abilities both to store optical energy at a higher density compared with other hosts and retrieve it efficiently. These glass are capable of hosting RE^{3+} ion doping due to their low refractive index, low melting point, low dispersion, and high transparency in addition to their outstanding thermo-optical characteristics.[6] Additionally, they have multiple applications in optical data transfer, laser

processing detection, and sensing. Infusing activator ions, such as rare-earth ions, can improve the strength, toughness, and luminescence effectiveness of host materials.[7,8] RE ions, such as Eu^{3+}, have narrow and monochromatic emission spectra, making them one of the greatest prospects for photonic applications as phosphors in field-emission technology. The $^7F_2$ transition at ~612 nm has both a narrow and monochromatic emission spectrum. At room temperature, spectral holes can be burned in the $^7F_0 \rightarrow {}^5D_0$ transition, which could be beneficial for high-density optical storage.[9] RE^{3+} ion kinetics, which is influenced by their interaction with the host material, typically limits the luminescence of these Eu^{3+}-doped materials.

Phosphate glass has excellent thermal stability, low melting and flexible structures and softening temperatures.[10] It also possesses a moderate phonon energy level, as well as low dispersion and excellent ultraviolet (UV) light transmittance.[11] Therefore, phosphate glass is one of the best materials for RE^{3+} ion doping due to its excellent properties. High-concentration phosphate glass with high Bi_2O_3 content have been used widely for optical applications because of their high nonlinearity. The SrF_2 compounds have a wide range of transparency from 0.15–11 μm, reduced phonon energy, and lower spectral dispersion. Additionally, SrF_2 can also improve the clarity of glass while lowering its thermal performance. There have, however, not been any extensive studies examining the optical properties of phosphate glass doped with bismuth oxide or strontium fluoride. Taking these factors into account, the primary purpose of this research was to invent a new type of phosphate glass (PBNSEu) doped with different concentrations of Eu^{3+} ions and to study and evaluate the J–O parameters, radiative properties, stimulated emission cross-section, and radiative lifetime. The concentration quenching effect on photoluminescence properties was examined.

2 | EXPERIMENTAL

2.1 | Glass preparation

The melt-quenching method was used to make bismuth-based phosphate glass doped with Eu^{3+} ions. The glass chemicals used in the current research work are given below. All reactive gradient chemicals were prepared by HiMedia with a purity level of 99.9%. The current glass chemical equations are given below:

1. $60.0\ P_2O_5 + 20\ Bi_2O_3 + 10\ Na_2CO_3 + 10SrF_2$
2. $59.9\ P_2O_5 + 20\ Bi_2O_3 + 10\ Na_2CO_3 + 10SrF_2 + 0.1\ Eu_2O_3$
3. $59.5\ P_2O_5 + 20\ Bi_2O_3 + 10\ Na_2CO_3 + 10SrF_2 + 0.5\ Eu_2O_3$
4. $59.0\ P_2O_5 + 20\ Bi_2O_3 + 10\ Na_2CO_3 + 10SrF_2 + 1.0\ Eu_2O_3$
5. $58.5\ P_2O_5 + 20\ Bi_2O_3 + 10\ Na_2CO_3 + 10SrF_2 + 1.5\ Eu_2O_3$
6. $58.0\ P_2O_5 + 20\ Bi_2O_3 + 10\ Na_2CO_3 + 10SrF_2 + 2.0\ Eu_2O_3$

The reagent-grade raw chemical compounds used were P_2O_5, Bi_2O_3, Na_2CO_3, SrF_2, and Eu_2O_3; a 20 g mixture was prepared. The raw materials were weighed and the chemicals were placed in an agate motor and crushed thoroughly, an alumina crucible was used to hold the homogeneous mixture, and then placed in an electric furnace and heated at 1100°C for 1.5 h. Next, the melted liquid was poured onto a preheated brass plate, and then annealed at 400°C for 10 h, and cooled to room temperature to remove the residual internal thermal stress in the glass. The prepared glass samples were polished to an average thickness (2 mm) for optical measurements. The polished samples are shown in Figure 1. The prepared samples were labelled PBNSEu01, PBNSEu05, PBNSEu10, PBNSEu15, and PBNSEu20 corresponding to 0.1, 0.5, 1.0, 1.5 and 2.0 mol%, respectively, of Eu^{3+} ions.

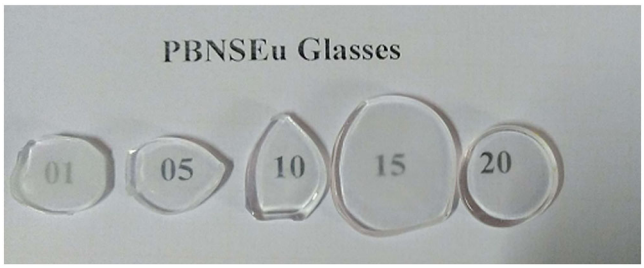

FIGURE 1 Polished PBNSEu glass samples

2.2 | Experimental techniques

Using a RIGAKU X-ray diffractometer, the XRD spectrum of a PBNSEu20 sample was recorded in the range 10–80^0. EDAX spectroscopy (Oxford INCA Penta FETX3) was used to identify the elemental analysis of this glass system. The prepared sample refractive index (n) and density ('ρ') were measured using an Abbe refractometer (with $C_{10}H_7Br$ as the contact liquid) and Archimedes' principle (with distilled water as the dipping liquid). An FTIR spectrometer (Bruker Alpha-II) was used to study the various bonds in the PBNSEu glass in the spectral region between 4000 and 600 cm^{-1}, with a resolution of 2 cm^{-1}. The absorption spectra were recorded in the wavelength range 300–2000 nm with a resolution of 1 nm using a JASCO model V-570 ultraviolet–visible–near-infrared (UV–vis–NIR) spectrometer. An FLS-980 fluorolog-3 spectrophotometer was used to record the excitation and emission spectra for all manufactured glass samples. The trials were all carried out at room temperature (RT).

3 | RESULTS AND DISCUSSION

3.1 | Physical parameters

Different physical factors were assessed for the fabricated Eu^{3+}-doped bismuth oxide–sodium carbonate–phosphate glass (PBNSEu) using equations reported in the literature,[12] which included the refraction index (n), density (g/cm^3), polaron radius (r_p [Å]), thickness (cm), Eu_2O_3 ion concentration (ions/cm^3), interatomic distance within Eu^{3+} ions (r_i, Å), filed strength ($F \times 10^{-14}$, cm^2), loss of reflection (%),

and electronic polarizability ($\times$ 10^{24} cm^3), the evaluated physical parameter values are presented in Table 1. From Table 1, it was observed that when the concentrations of Eu^{3+} ions were increased, the glass density and refractive index values increased slightly from PBNSEu01 to PBNSEu20, because, at high concentrations, europium ions are very close to each other and very compactly placed. In this case, as the dopant concentration was increased, the molar volume and interionic distance values dropped, indicating that the atoms in the produced glass were tightly bound.

3.2 | XRD spectra analysis

Figure 2 shows the XRD spectra recorded in the range 10–80°. The XRD spectra of the PBNSEu20 glass powder, which can be seen in Figure 2, did not show any crystalline peak, clearly indicating the non-crystalline nature. The fabricated PBNSEu20 glass sample is amorphous.

3.3 | EDAX spectra analysis

The EDAX spectra of the manufactured PBNSEu20 glass powder are shown in Figure 3. This showed the successful inclusion of constituents such as elements into the host matrix. The presence of P, Na, O, Bi, Sr, and Eu components in the investigated glass system was confirmed using these spectra.[13]

3.4 | FT-TR spectra analysis

Based on Zachariasen,[14] Van Wazer,[15] and Flory,[16] phosphate glass consist of a network of polymeric structures that are controlled by the glass composition. PO_4 tetrahedra are the dominant structures in this network. A terminal double-bonded oxygen atom (DBO) resides in one of the four vertices of vitreous P_2O_5's groups that are connected to other units by three of its four vertices. Figure 4 depicts the FTIR spectra of the fabricated PBNSEu20 glass. This process involves infrared (IR) photons engaging with molecules to excite them to a higher energy state. As shown in Figure 4, data from the glass doped with Eu^{3+} ions were captured between 600 and 4000 cm^{-1} to gather proof from the structural and sensitive group analyses. The IR spectrum at 690 cm^{-1} demonstrates that the bending vibration of the prepared glass was due to the P–O–P group, the absorption peak at 850 cm^{-1} corresponds to the stretching vibration of the strong bending group C–H, and 1150 cm^{-1} the asymmetrical stretching modes of the PO_4 groups. The absorption peak at 1250 cm^{-1} presents symmetric stretching vibrations of P═O bonds. For the corresponding element groups in the phosphate glass system, these bands have their elementary characteristic vibration wave numbers.[17,18]

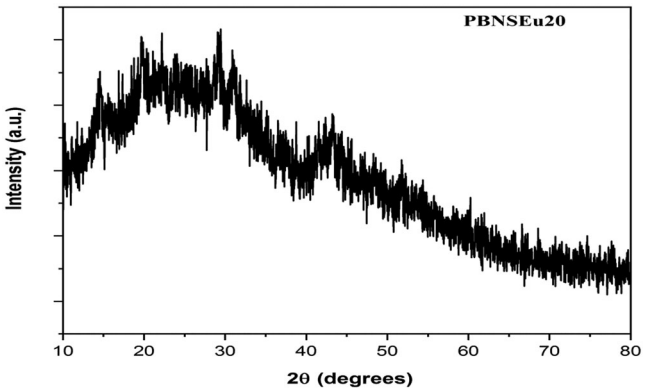

FIGURE 2 XRD spectrum of PBNSEu20 glass

TABLE 1 Physical parameters of PBNSEu glass

Physical properties	PBNSEu01	PBNSEu05	PBNSEu10	PBNSEu15	PBNSEu20
Thickness (cm)	0.301	0.302	0.304	0.305	0.306
Density (g/cm^3)	3.505	3.511	4.527	4.535	4.608
Dielectric constant (ϵ)	2.732	2.735	2.742	2.745	2.748
Refractive index (n)	1.653	1.654	1.656	1.657	1.658
Concentration N (mol/lit)	0.012	0.061	0.157	0.183	0.282
Molar volume V_m (cm^3/mol)	69.311	69.285	53.806	53.792	53.010
Concentration N (ions/c.c $\times$ 10^{20})	0.146	0.737	1.896	2.207	3.402
Electronic polarizability ($\times 10^{-24}$ cm^3)	10.052	10.061	7.832	7.839	7.734
Field strength F ($\times$ 10^{-14} cm^{-2})	1.107	3.264	6.096	6.745	9.000
Optical dielectric constant (ϵ_{opt})	1.729	1.732	1.732	1.732	1.732
Interionic distance R_i (Å)	40.827	23.850	17.404	16.545	14.234
Metalization factor M	0.634	0.634	0.634	0.635	0.634
Polaran radius R_p (Å)	16.455	9.613	7.014	6.668	5.773
Molar refractivity (cm^{-3})	25.373	25.394	19.768	19.787	19.522

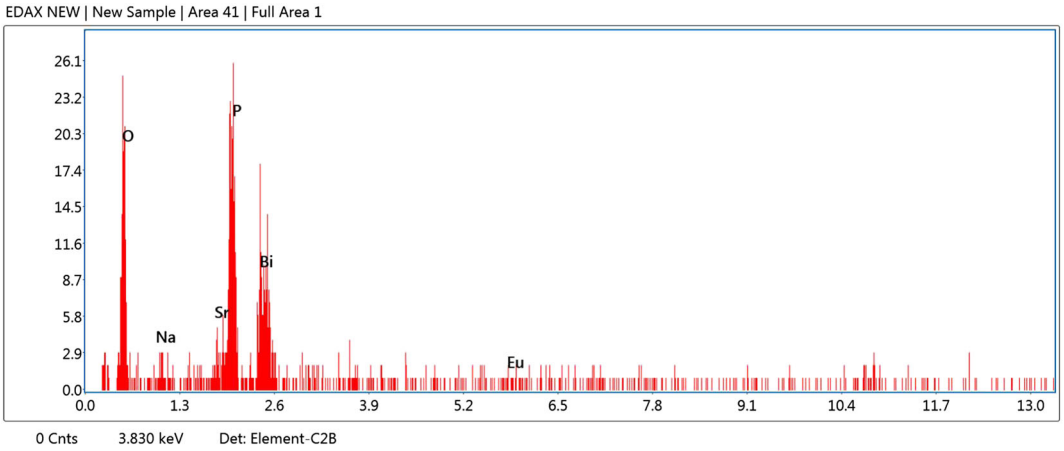

FIGURE 3 EDAX spectrum of PBNSEu20 glass

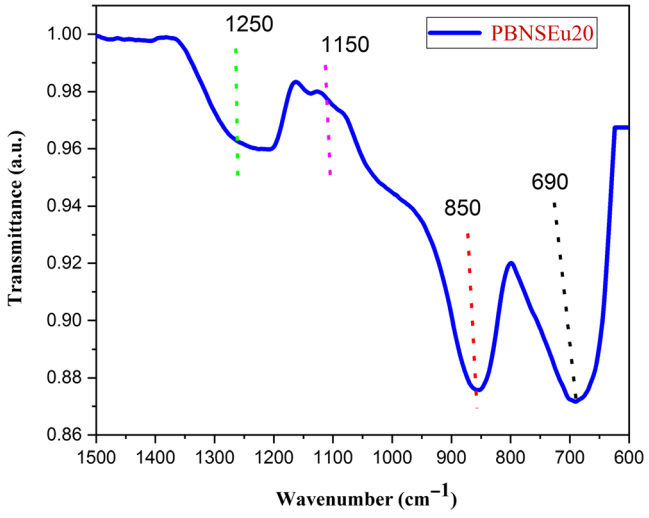

FIGURE 4 FTIR spectrum of PBNSEu20 glass

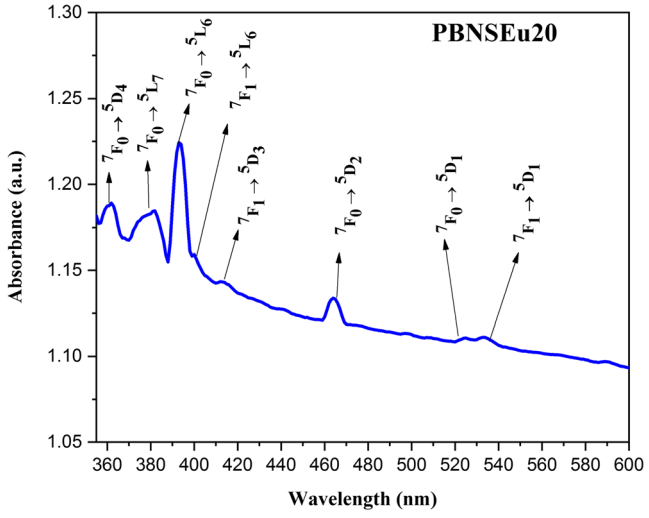

FIGURE 5 Optical absorption spectrum of PBNSEu20 glass

3.5 | Absorption spectra

The optical absorption spectrum (range 350–600 nm) of PBNSEu glass doped with 2.0 mol% Eu^{3+} ions is shown in Figure 5. The absorption spectra show in total, eight absorption peaks centred at 361, 382, 394, 402, 412, 465, 525 and 535 nm and the corresponding transitions $^7F_0 \rightarrow {}^5D_4$, $^7F_0 \rightarrow {}^5L_7$, $^7F_0 \rightarrow {}^5L_6$, $^7F_1 \rightarrow {}^5L_6$, $^7F_1 \rightarrow {}^5D_3$, $^7F_0 \rightarrow {}^5D_2$, $^7F_0 \rightarrow {}^5D_1$, and $^7F_1 \rightarrow {}^5D_1$, respectively, due to the Carnall intra 4f transitions of Eu^{3+} ions[19], and were used to assign these spectral transitions and their signifying band locations, which were identical, as described previously.[20–24] Among the trivalent RE ions, only the Eu^{3+} ions exhibited two thermally occupied ground states ($^7F_0$ and $^7F_1$). In host materials doped with Eu^{3+} ions, absorption transitions from both the $^7F_0$ (ground state) and $^7F_1$ (thermally filled state) occurred due to the smaller energy difference (360 cm^{-1}) between these levels. Magnetic dipoles were allowed in the $^7F_0 \rightarrow {}^5D_1$ and $^7F_1 \rightarrow {}^5D_1$ transitions, among those detected. As it adheres to the selection criteria $\Delta L \leq 2$, and $\Delta J \leq 2$, the $^7F_0 \rightarrow {}^5D_2$ transition is regarded as a hypersensitive peak.

3.6 | Optical band gap analysis

An optical band gap is a critical parameter in determining the current flow (carrier generation and recombination) in solid-state physics. An optical absorption spectrum can be used to measure the optical band gap, which is the energy difference between the valence band and conduction band of the glass samples. The information it provides about the material is critical for understanding its characteristics. As a result of Tauc's plots, the direct and indirect energy band gaps and Urbach energy (ΔE) were analyzed, as shown in Figure 6(a–c). Specifically, the values for the direct band gaps ($n = 1/2$) were between 3.77 and 4.16 eV, whereas those for the indirect band gaps ($n = 2$) were between 4.10 and 4.27 eV. These values are listed in Table 2 and compared with published results. There is considerable evidence that trivalent oxides can depolarize a

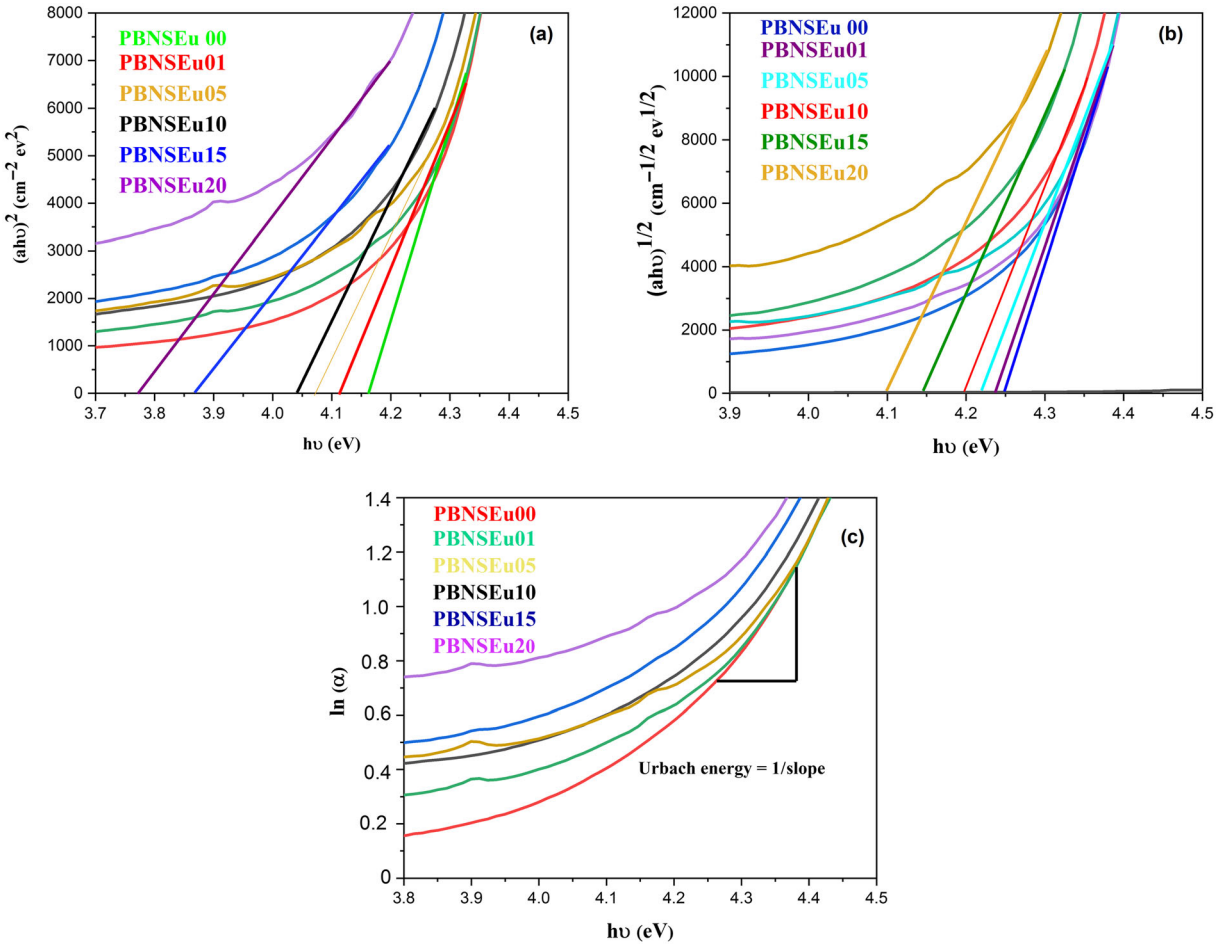

FIGURE 6 (a) Direct band gap energy; (b) indirect band gap energy; and (c) Urbach energy of PBNSEu glass

TABLE 2 Optical band gap values of PBNSEu glass (a) direct (b) indirect (c) Urbach energy

Glass samples	Direct band gap (eV)	Indirect band gap (eV)	Urbach energy (eV)	References
PBNSEu00	4.16	4.27	0.21	[This work]
PBNSEu01	4.11	4.23	0.26	[This work]
PBNSEu05	4.07	4.22	0.34	[This work]
PBNSEu10	4.04	4.19	0.37	[This work]
PBNSEu15	3.86	4.14	0.36	[This work]
PBNSEu20	3.77	4.10	0.49	[This work]
0.1EuKTTB	3.314	3.167	0.51	[24]
0.3EuKTTB	3.290	3.134	0.52	[24]
0.5EuKTTB	3.262	3.092	0.54	[24]
1EuKTTB	3.235	3.072	0.60	[24]
2EuKTTB	3.211	3.053	0.80	[24]

glass-forming system, thereby altering the oxygen bonding in the network, and altering the absorption characteristics. When the absorption band shifts to higher energies, there are fewer oxygen molecules, making the structure more compact by reducing the number of nonbridging oxygen molecules. The band gap values of PBNSEu glass were altered with the increase in the concentration of Eu^{3+} ions due to the structural modification and nonbridging oxygen (NBO) forming in the network.[25,26] As the band gap value is inversely correlated with the Urbach energy value, this indicates the level of defects in the prepared glass. A tail of energy near the

TABLE 3 The PBNSEu glass, comparison of J–O parameters ($\Omega_\lambda \times 10^{-20}$ cm^2)

Glass host	Ω_2 ($\times 10^{-20}$ cm^2)	Ω_4 ($\times 10^{-20}$ cm^2)	Ref.
PBNS:01Eu^{3+}	3.44	1.07	[This work]
PBNS:05Eu^{3+}	3.50	1.16	[This work]
PBNS:10Eu^{3+}	3.70	1.20	[This work]
PBNS:15Eu^{3+}	3.82	1.21	[This work]
PBNS:20Eu^{3+}	3.87	1.22	[This work]
SABiBEu10	5.00	1.13	[13]
SABiBEu15	4.40	1.14	[13]
SBNCEu15	5.50	4.01	[30]
PKALCaF	3.64	0.27	[31]
TeEu1.0	5.95	4.52	[32]
TeEu1.5	6.22	5.01	[32]
Fluorophosphate	3.24	5.11	[33]
Oxyfluoroborate	3.45	2.93	[34]
LNaFB	3.62	1.43	[35]
TFBLN	6.92	3.40	[36]

absorption coefficient and optical band edge is known as Urbach's energy band.[27] Plotting $ln\alpha$ vs photon energy ($h\upsilon$) with their inverse slopes gives the ΔE value, and an empirical expression is presented here as $\alpha(v) = \alpha 0$ exp ($h\upsilon$ ΔE). Band gap measurements revealed the values for PBNSEu00 (0.21 eV), PBNSEu01 (0.26 eV), PBNSEu05 (0.34 eV), PBNSEu10 (0.37 eV), PBNSEu15 (0.39 eV), and PBNSEu20 (0.49 eV) listed and in Table 2 compared with published results.[24]

3.7 | Judd–Ofelt intensity parameters

In the present work, the J–O intensity parameters were calculated using emission spectral transitions $^5D_0 \rightarrow {}^7F_2$, $^7F_4$ and $^7F_0$ of Eu^{3+} ion-doped PBNS glass and related equations[28,29] were used to evaluate the JO intensity parameters. The parameters Ω_2 and Ω_4 were calculated in the current work and the values are presented in Table 3[13,30–36]; these values were compared with other reported glass. As the transition $^5D_0 \rightarrow {}^7F_5$ cannot be observed in the emission spectrum, the intensity parameter Ω_6 has not been evaluated. The trend of the J–O intensity parameters ($\Omega_2 > \Omega_4$) indicates the covalence and asymmetry around the rare-earth ions with their ligand fields.[37] In the present work, the Ω_2 value was been increased from 0.1 mol% to 2.0 mol% Eu^{3+} ions. PBNSEu20 glass has a higher Ω_2 ($= 3.87 \times 10^{-20}$ cm^2) value, which indicates that the prepared glass had a higher covalence (low iconicity). The Ω_4 value ($= 1.22 \times 10^{-20}$ cm^2) parameter increased from PBNSEu01 to PBNSEu20 mol%, and followed the trend of $\Omega_2 > \Omega_4$. The high value of the intensity parameter Ω_4 of the PBNSEu20 glass indicates the high rigidity of the glass matrix, the small variation in these J–O parameters mostly depended on host selection and concentration quenching effect.

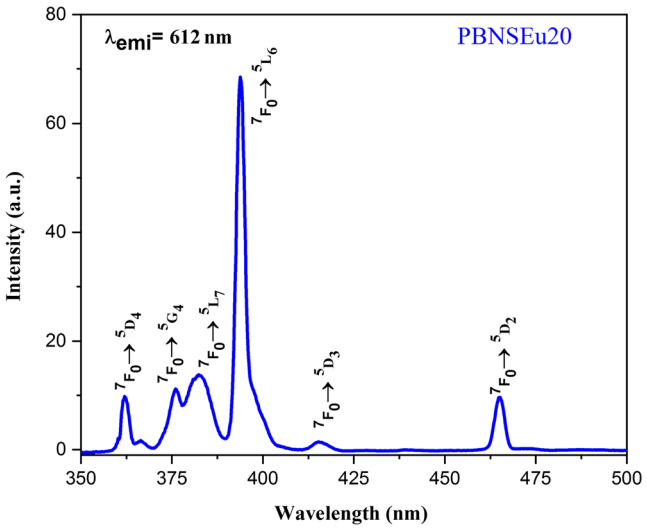

FIGURE 7 Fluorescence excitation spectrum of Eu^{3+} ion-doped PBNS glass

3.8 | Excitation and emission analysis

As a result, λ_{emi} was adjusted to 612 nm in the current investigation to record the excitation spectra in the 350–500 nm region of the PBNSEu20 glass, as shown in Figure 7. Figure 7 depicts six excitation bands at 362, 375, 382, 394, 415, and 465 nm, which are related to the lower energy state $^7F_0$ and some high energy states, including $^5D_4$, $^5G_4$,$^5L_7$, $^5L_6$, $^5D_3$, and 5D2. The wavelength (394 nm) that corresponded to this $^7F_0 \rightarrow {}^5L_6$ transition was utilized to stimulate the PBNSEu glass to record the emission spectra, because the maximum intensity was obtained at this transition.[13]

Figure 8 shows the room-temperature emission spectra of the PBNSEu glass that were investigated in the spectral range 560–720 nm. The excitation wavelength used to capture the fluorescence emission spectra was 394 nm. In Figure 8, five emission peak positions are found at 578, 592, 612 and 653 nm, and 702 nm; the related transitions are 578 nm ($^5D_0 \rightarrow {}^7F_0$), 592 nm ($^5D_0 \rightarrow {}^7F_1$), 612 nm ($^5D_0 \rightarrow {}^7F_2$) 653 nm ($^5D_0 \rightarrow {}^7F_3$) and 702 nm ($^5D_0 \rightarrow {}^7F_4$), respectively. The transition $^5D_0 \rightarrow {}^7F_2$ (612 nm) was determined to have the highest intensity peak of all transitions. Here we observed that, with increasing Eu^{3+} ions concentration, the intensity of the emission peak increased from 1.0 to 2.0 mol%. The interionic distance between the europium ions decreased as the concentration of Eu_2O_3 ions was increased; this was caused by the cross-relaxation energy transfer of the Eu^{3+} ion concentration. The calculated values were PBNSEu01 (40.82 Å), PBNSEu05 (23.85 Å) PBNSEu10 (17.40 Å), PBNSEu15 (16.54 Å), and PBNSEu20 (14.23 Å).[30]

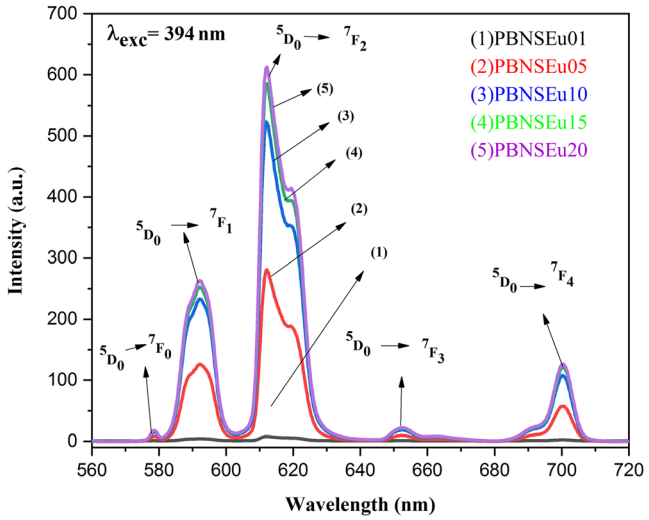

FIGURE 8 Fluorescence emission spectra of Eu^{3+} ion-doped PBNS glasses

3.9 | Partial energy level diagram of Eu_2O_3 ion-doped PBNS glass

Analysis of the partial energy level structure of the Eu^{3+} ions is shown in Figure 9, which depicts the transitions of the Eu^{3+} ion in the PBNS glass. In the excitation spectra, the highest intensity excitation peak was observed at 394 nm and corresponded to the electron transition $^7F_0 \rightarrow {}^5L_6$. With a 394 nm excitation source from the xenon lamp, the

TABLE 4 Radiative parameters such as band position (λ_p, nm), effective bandwidth ($\Delta\lambda_{eff}$, nm), radiative transition probabilities (A_R, S^{-1}), stimulated emission cross-section ($\sigma_{emi} \times 10^{-22}$ cm^2), and experimental branching ratios (β_R) for $^5D_0 \rightarrow {}^7F_{J\ (J=0,1,2,3,4)}$ PBNSEu20 glass

Transition	λ_P	$\Delta\lambda_{eff}$	A_R	σ_{emi}	β	
					β_{exp}	β_{cal}
$^5D_0 \rightarrow {}^7F_0$	578	0.40	0.00	0.00	0.00	0.00
$^5D_0 \rightarrow {}^7F_1$	592	10.06	64.19	4.12	0.25	0.25
$^5D_0 \rightarrow {}^7F_2$	612	10.14	160.60	11.69	0.64	0.64
$^5D_0 \rightarrow {}^7F_3$	653	0.60	0.00	0.00	0.00	0.00
$^5D_0 \rightarrow {}^7F_4$	702	6.52	25.25	4.95	0.10	0.10

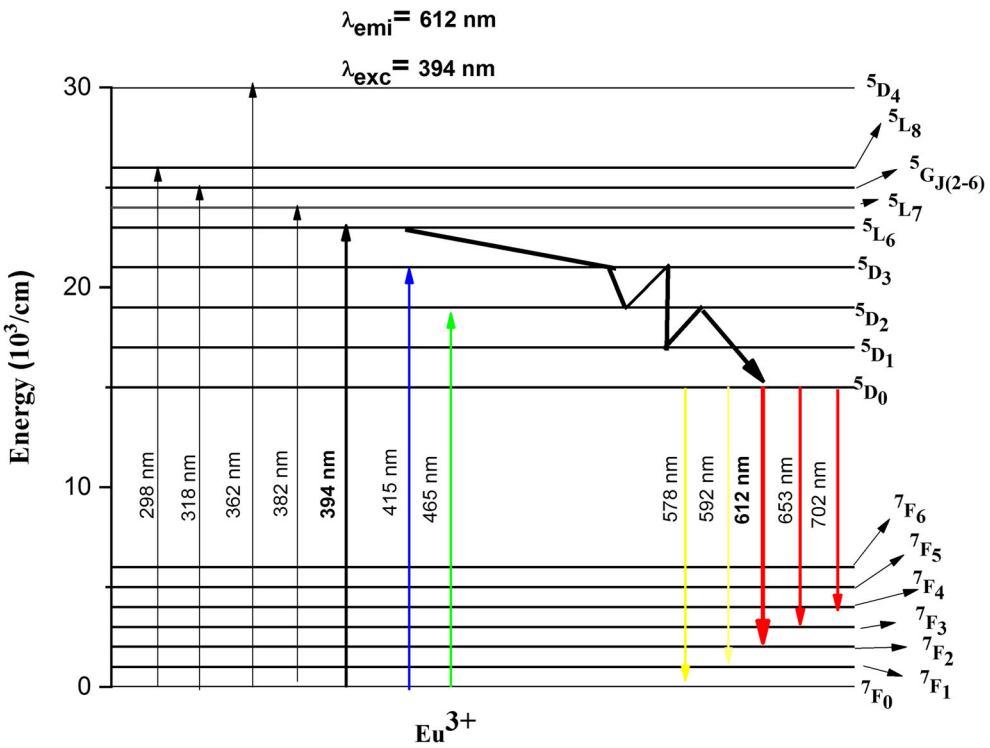

FIGURE 9 Partial energy level diagram of the PBNSEu glass system

TABLE 5 Emission band position (λ_p, nm), optical gain ($\sigma_{emi} \times \tau_{exp} \times 10^{-25}$ cm^2 S), effective bandwidth ($\Delta\lambda_{eff}$, nm), radiative transition probabilities (A_R, S^{-1}), peak stimulated emission cross-section ($\sigma_{emi} \times 10^{-22}$ cm^2), and experimental branching ratio (β_R) for transitions of Eu^{3+} ions in PBNS glass

Transitions $^5D_0 \rightarrow$	Parameters	PBNSEu01	PBNSEu05	PBNSEu10	PBNSEu15	PBNSEu20
$^7F_1$	λ_P	592	592	592	592	592
	$\Delta\lambda_{eff}$	10.03	7.79	8.26	10.27	10.06
	A_R	64.31	64.31	64.31	64.19	64.19
	σ_{emi}	4.14	5.33	5.03	4.04	4.12
	β_{exp}	0.26	0.27	0.26	028	0.25
	$\sigma_{emi} \times \Delta\lambda_{eff}$	42.64	41.52	41.54	41.49	41.44
$^7F_2$	λ_P	612	612	612	612	612
	$\Delta\lambda_{eff}$	11.59	9.42	9.32	0.43	10.14
	A_R	160.82	147.35	155.77	144.53	160.60
	σ_{emi}	10.64	11.55	12.33	10.22	11.69
	β_{exp}	0.64	0.62	0.63	0.63	0.64
	$\sigma_{emi} \times \Delta\lambda_{eff}$	123.31	108.80	114.91	106.59	118.53
	A_T	249	235	245	231	252
	τ_{cal}	4.00	4.25	4.07	4.32	3.96
$^7F_4$	λ_P	702	702	702	702	702
	$\Delta\lambda_{eff}$	5.79	6.21	10.43	7.08	6.52
	A_R	24.46	23.61	25.51	25.51	25.25
	σ_{emi}	5.39	4.86	3.12	4.60	4.95
	β_{exp}	0.09	0.10	0.10	0.09	0.10
	$\sigma_{emi} \times \Delta\lambda_{eff}$	31.20	30.18	32.54	32.56	32.27

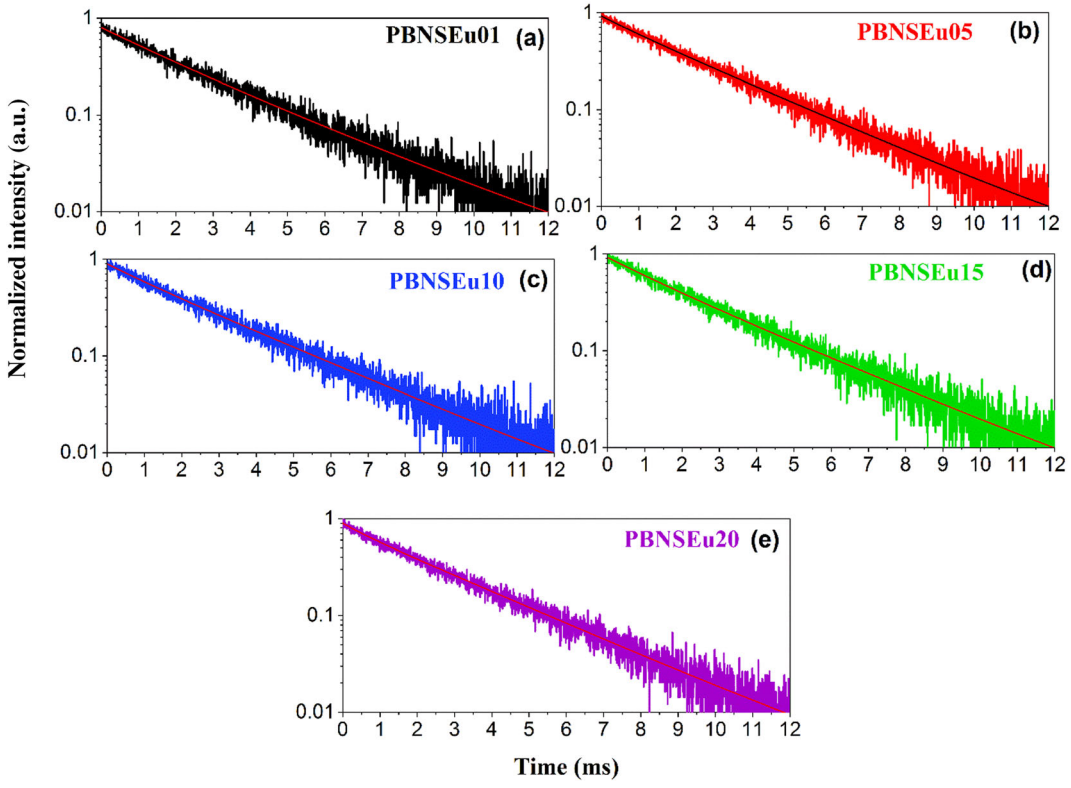

FIGURE 10 (a–e) Fluorescence decay profiles of PBNSEu glass

electrons in the $^7F_0$ ground state absorb sufficient energy to be excited to the $^5L_6$ level, which drops to the $^5D_0$ level using the nonradiative (NR) relaxation channel and then radiates to the lowest energy levels ^7F_J (where J = 0, 1, 2, 3 and 4), causing the emissions in the visible region.[38] In the current work, the emission intensity at ~612 nm ($^5D_0 \rightarrow {}^7F_2$) was the highest, when compared with the other transitions.

3.10 | Radiative properties

Various radiative parameters, such as the probability of radiative transition (A_R) and the total radiation transition rate (A_τ), branching ratio (β_R), and the radiation lifetime (τ_R), were evaluated for all PBNSEu glass by following the equations[13] and radiative factors detailed in Table 4. These radiative parameters were obtained from the emission spectra; radiative parameters such as σ_{emi} (stimulated emission cross-section), wavelength (λ_p), gain bandwidth ($\sigma_{emi} \times \Delta\lambda_{eff}$), effective bandwidth ($\Delta\lambda_{eff}$), experimental branching ratio (β_{exp}), and optical gain parameters ($\sigma_{emi} \times \tau_R$) were calculated for the fabricated PBNSEu glass, and the resulting values are shown in Table 5. It can be seen from Table 5 that the emission parameters of the PBNSEu20 glass had reached a higher value. The PBNSEu20 glass (optimized glass) obtained values were optical gain parameters ($\sigma_{emi} \times \tau_R = 295.17 \times 10^{-25}$ cm^2 S), bandwidth gain ($\sigma_{emi} \times \Delta\lambda_{eff} = 118.53 \times 10^{-25}$ cm^3), stimulated emission cross-section ($\sigma_{emi} = 11.69 \times 10^{-20}$ cm^2), and branching ratio (0.64) for this transition $^5D_0 \rightarrow {}^7F_2$. For the design and development of low threshold and high gain laser applications, the higher stimulated emission cross-section is one appealing aspect. The experimental branching ratios found for the PBNSEu glass and larger values for the stimulated emission cross-section are used to produce visible display device lasers. The luminescence branching ratio is another crucial measure to quantify laser power.

TABLE 6 Measured and calculated lifetime values and quantum efficiency (η (%)) of the fabricated PBNSEu glasses

Glass sample	τ_{exp} (ms)	τ_R (ms)	η (%)	Ref.
PBNSEu01	2.564	4.000	64.10	[This work]
PBNSEu05	2.592	4.250	60.98	[This work]
PBNSEu10	2.575	4.071	63.25	[This work]
PBNSEu15	2.545	4.324	58.85	[This work]
PBNSEu20	2.445	3.967	61.63	[This work]

TABLE 7 CIE colour coordinates and CCT values of the prepared PBNSEu glass

Glass samples	Colour coordinates		CCT (K)	References
	x	y		
PBNSEu01	0.603	0.314	2611	[This work]
PBNSEu05	0.609	0.310	2750	[This work]
PBNSEu10	0.655	0.254	4633	[This work]
PBNSEu15	0.661	0.264	5760	[This work]
PBNSEu20	0.671	0.278	5781	[This work]
Eu0.25	0.625	0.374	1191	[42]
Eu0.75	0.646	0.354	2499	[42]
Eu1	0.644	0.356	2342	[42]
BTC2E	0.645	0.354	2228	[43]
KZPEu	0.637	0.351	2117	[44]

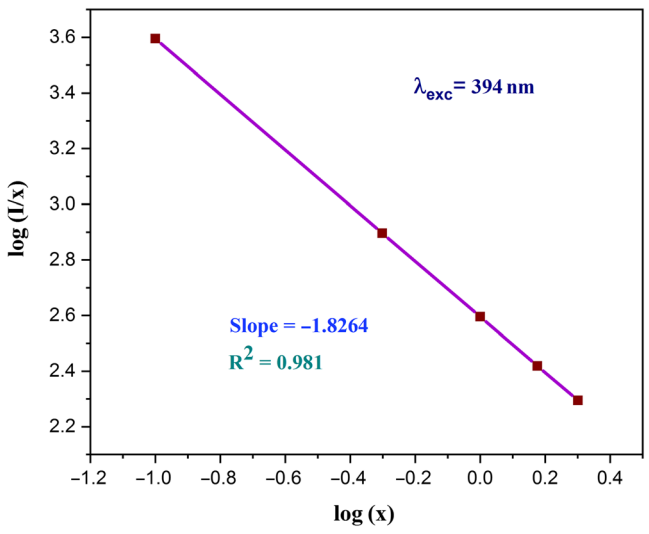

FIGURE 11 Concentration quenching effect between Eu^{3+} ions in PBNS glass

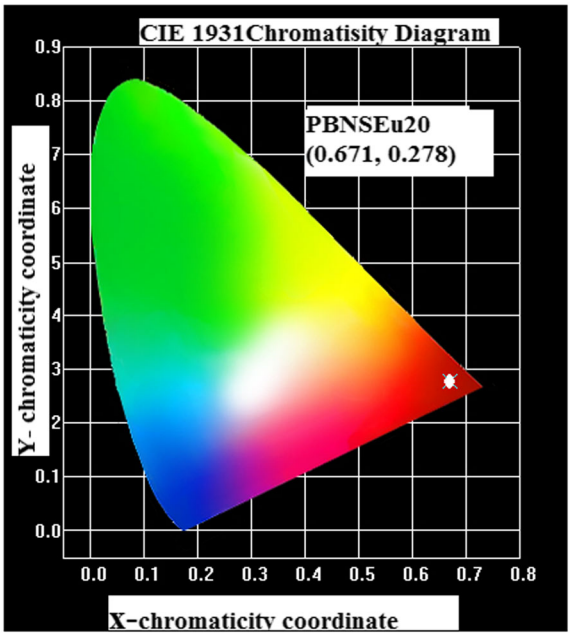

FIGURE 12 1931 CIE chromaticity colour coordinates of the PBNSEu20 glass

3.11 | Photoluminescence lifetime decay analysis

One of the crucial factors in the design and production of RE-doped materials for real-time applications, such as optical amplifiers, contemporary laser technologies, etc., is the fluorescence lifetime of an excited energy state of RE ions. Figure 10(a–e) depicts the fluorescence decay trend for the PBNSEu glass that was seen when the $^5D_0$ energy level of Eu^{3+} ions was excited at 394 nm. For all europium ion concentrations in PBNS glass, the decay profiles were well matched to a single exponential. Table 6 lists the results of the calculations carried out to determine lifetime and quantum efficiency values using the equations listed previously.[30] Due to energy transfer between Eu^{3+} ions at higher concentrations of Eu^{3+} ions, the fluorescence lifetime values of the $^5D_0$ excited level PBNS glass decreased as the Eu^{3+} ion concentration was increased. According to Table 6, the PBNSEu01 glass has a better quantum efficiency (64.1%) than the remaining concentrations.

The relationship between log (I/x) and log (x) was explored using the following formula to calculate the energy transfer mechanism between Eu^{3+} ions in PBNSEu phosphate glass[39,40]:

$$\log (I/x) = A - (\theta/3) \log x \quad (1)$$

where I stand for emission intensity, x for doping concentration, A for constant, and θ = 6, 8, and 10 for dipole–dipole, dipole–quadrupole, and quadrupole–quadrupole interactions, respectively. The relationship between log(I/x) and log(x) is shown in Figure 11, and the fitted straight line exhibited a slope of −1.826. The θ value was then determined to be 5.479. This value was very close to 6, so the concentration quenching mechanism of PBNSEu was through a dipole–dipole interaction.

3.12 | CIE and CCT parameters

The Commission Internationale de l'éclairage – 1931 (CIE-1931) chromaticity coordinates were used to assess the actual colour of the studied PBNSEu glass. Using the formula detailed in the literature, colour coordinates (x, y) for chromaticity were computed using emission data.[41–44] The CIE standard reference for identifying visible colours of human eyes, particularly the borders of the CIE diagram corresponded to monochromatic light. The CIE coordinate values for the PBNSEu glass were evaluated, and the results are displayed in Table 7. Figure 12 shows that the values fell into the red-emission region. The generated europium-doped PBNS glass emitted red emission at the 394 nm excitation wavelength, according to the colour coordinate values of optimized PBNSEu20 (0.671, 0.278) glass and equivalent values in Table 7. The correlated colour temperature (CCT) values were calculated using the equation from previous reports.[45] PBNSEu01 (2611 K), PBNSEu05 (2750 K), PBNSEu10 (4633 K), PBNSEu15 (5760 K), and PBNSEu20 (5781 K) were the acquired CCT values. These obtained values were good when compared with BTC2E (2228 K)[43] and KZPEu (2117 K).[44]

3.13 | Temperature-dependent luminescence studies

Temperature-dependent luminescence spectra were obtained under an excitation wavelength (λ_{exi} = 394 nm) at various temperatures ranging from RT (303 K) to 453 K, to investigate the effect of temperature on the emission profile. Figure 13(a) depicts the temperature-dependent luminescence of the PBNSEu20 glass. The emission peak intensities decreased with increasing temperature for PBNSEu20 glass, as shown in Figure 13(a). At 423 K, the emission intensity dropped to 86.65%, and at 453 K, it dropped to 79.98%, demonstrating that Eu^{3+}-triggered PBNSEu20 glass is thermally stabile. Furthermore, the activation energy (ΔE) determined for the PBNSEu20 glass thermal performance was good. As a result, the activation energy was calculated using the Arrhenius equation[46,47] based on the relationship between temperature and emission intensity. The activation energy was determined by the slope of the linear fit graph between ln

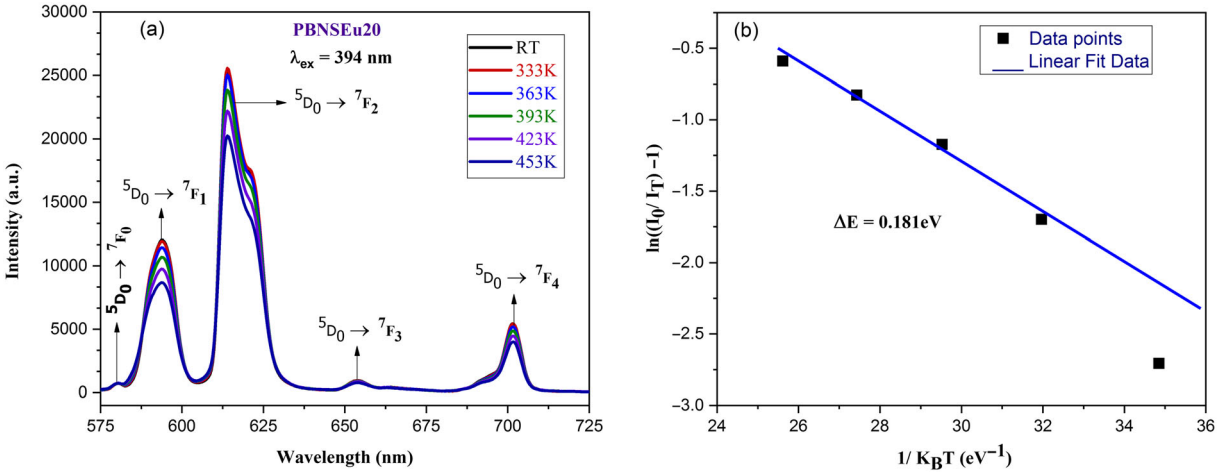

FIGURE 13 (a) Temperature-dependent luminescence emission intensity spectra for PBNSEu20 glass. (b) Linear relationship of $ln([I_0/I_T]-1)$ versus $1/K_BT$ graph

($[I_0/I_T]$ -1) and $1/K_{BT}$, as illustrated in Figure 13(b). Therefore, it was found that the ΔE of PBNSEu20 glass was 0.181 eV, which compared with previously reported values.[48] The produced PBNSEu20 glass sample had exceptional thermal stability, as evidenced by the high activation energy value.

4 | CONCLUSION

In the current study, activated phosphate glass (PBNSEu) were prepared using the well known melt-quenching technique, and with different Eu^{3+} ion concentrations. The physical, structural, optical, and photoluminescence characteristics were analyzed. The XRD pattern confirmed the fabricated PBNSEu glass as having a noncrystalline nature. The presence of the elements P, Na, O, Bi, Sr, and Eu in the studied glass was recognized using EDAX spectroscopy. The developed PBNSEu glass contained several functional groups and linkages, which were validated using FTIR spectroscopy. Using the J–O theory, the intensity parameters (Ω_2, Ω_4) were calculated from the emission spectra and followed the $\Omega_2 > \Omega_4$ trend. The PBNSEu20 glass had a maximum emission intensity for the $^5D_0 \rightarrow {}^7F_2$ transition (612 nm) compared with other transitions. The obtained five emission transitions of the $^5D_0 \rightarrow {}^7F_2$ (612 nm) transition spectral characteristics values were optical gain parameters ($\sigma_{emi} \times \tau_R = 295.17 \times 10^{-25}$ cm^2S), stimulated emission cross-section ($\sigma_{emi} = 11.69 \times 10^{-22}$ cm^2), and gain bandwidth ($\sigma_{emi} \times \Delta\lambda_{eff} = 118.53 \times 10^{-25}$ cm^3) for the PBNSEu20 glass (optimized glass). The optical band gap values were calculated, and the lifetime values were evaluated for all concentrations of PBNSEu glass samples. According to the CIE chromaticity coordinates and CCT values, the PBNSEu glass emitted a noticeable red colour. The temperature-dependent luminescence and the activation energy were determined for the optimized PBNSEu20 glass sample. The obtained results strongly indicated that the PBNS glass doped with Eu^{3+} ions should be suitable for red LEDs, visible display laser applications, and w-LEDs.

ACKNOWLEDGEMENTS

The authors acknowledge the DST-Curie Centre, Sri Padmavati Mahila Visvavidyalayam, Tirupati, for extending the X-ray diffraction facility.

DECLARATION OF COMPETING INTEREST

The authors state that they have no known competing financial interests or personal relationships that may have influenced the work presented in this study.

DATA AVAILABILITY STATEMENT

The authors state that they have no known competing financial interests or personal relationships that may have influenced the work presented in this study.

ORCID

B. Deva Prasad Raju https://orcid.org/0000-0002-3485-1060

REFERENCES

[1] T. Hayakawa, M. Nogami, *J. Appl. Phys.* **2001**, *90*, 2200.
[2] F. Qu, N. O. Dantas, *Phys. B* **2003**, *327*, 79.
[3] M. J. Digonnet (Ed), *Rare earth doped fiber lasers and amplifiers*, Dekker, New York **1993**.
[4] V. A. Jerez, C. B. De Araujo, Y. Messaddeq, *J. Appl. Phys.* **2004**, *96*, 2530.
[5] M. J. Weber, *J. Non-Cryst. Solids* **1990**, *123*, 208.
[6] T. I. Suratwala, R. A. Steele, G. D. Wike, J. H. Campbell, K. Takenchi, *J. Non-Cryst. Solids* **2000**, *263*, 213.
[7] Q. Guanming, L. Xikum, Q. Tai, Z. Haitao, Y. Honghao, M. Ruiting, *J. Rare Earths* **2007**, *25*, 281.
[8] L. Yanhong, Z. Li, Y. Zhang, M. Jing, *J. Rare Earths* **2012**, *30*, 1195.
[9] V. Lavin, U. R. Rodriguez-Mendoza, I. R. Martin, V. D. Rodriguez, *J. Non-Cryst. Solids* **2003**, *319*, 200.
[10] L. Koudelka, P. Kalenda, J. Holubova, P. Mosner, L. Montagne, B. Revel, *J. Non-Cryst. Solids* **2017**, *476*, 114.
[11] B. Afef, M. M. Alqahtani, H. H. Hegazy, E. Yousef, K. Damak, R. Maalej, *J. Lumin.* **2018**, *194*, 706.
[12] P. Reddi Babu, N. Megala Rajesh, J. Sushma, B. Esra Kavaz, D. P. Raju, *Opt. Mater.* **2021**, *122*, 111725.
[13] M. Dhamodhara Naidu, D. Rajesh, A. Balakrishna, Y. C. Ratnakaram, *J. Rare Earths* **2014**, *32*, 1140.
[14] W. H. Zachariasen, *Am. Chem. Soc.* **1932**, *54*, 3841.
[15] J. R. Van Wazer, *J. Am. Chem. Soc.* **1950**, *72*, 644.
[16] P. I. Flory, *Principles of polymer chemistry*, Cornell University, Ithaca, NY **1953**.
[17] R. O. Omrani, S. Krimi, J. J. Videau, I. Khattech, E. A. Jazouli, M. Jemal, *J. Non-Cryst. Solids* **2014**, *390*, 5.
[18] S. S. Sastry, B. R. V. Rao, *Bull. Mater. Sci.* **2015**, *38*, 475.
[19] W. T. Carnall, P. R. Fields, K. Rajnak, *J. Chem. Phys.* **1968**, *49*, 4424.
[20] B. D. Prasad Raju, C. M. Reddy, *Opt. Mater.* **2012**, *34*, 1251.
[21] K. Annapoorani, K. Marimuthu, *J. Non-Cryst. Solids* **2017**, *463*, 148.
[22] M. Rajesh, M. R. Babu, N. J. Sushma, B. D. Prasad Raju, *J. Non-Cryst. Solids* **2019**, *528*, 119732.
[23] B. C. Jamalaiah, J. S. Kumar, A. M. Babu, L. R. Moorthy, *J. Alloys Compd.* **2009**, *478*, 63.
[24] K. Mariselvam, J. Liu, *J. Lumin.* **2021**, *230*, 117735.
[25] M. L. A. Letswalo, L. Reddy, A. Balakrishna, H. C. Swart, O. M. Ntwaeaborwa, *J. Lumin.* **2021**, *240*, 118462.
[26] M. Vijayakumar, K. Marimuthu, *J. Lumin.* **2016**, *178*, 414.
[27] F. Urbach, *Phys. Rev.* **1953**, *92*, 1324.
[28] B. R. Judd, *Phys. Rev.* **1962**, *127*, 750.
[29] G. S. Ofelt, *J. Chem. Phys.* **1962**, *37*, 511.
[30] M. Rajesh, G. R. Reddy, N. John Sushma, G. Devarajulu, B. D. P. Raju, *Opt. Mater.* **2020**, *107*, 110038.
[31] F. Zaman, J. Kaewkhao, G. Rooh, N. Srisittipokakun, H. J. Kim, *J. Alloys Compd.* **2016**, *676*, 275.
[32] W. Stambouli, H. Elhouichet, B. Gelloz, M. Ferid, *J. Lumin.* **2013**, *138*, 201.
[33] R. Balda, J. Fernandez, J. L. Adam, M. A. Arriandiaga, *Phys. Rev. B* **1996**, *54*, 12076.
[34] Y. Dwivedi, S. B. Rai, *Opt. Mater.* **2008**, *31*, 87.
[35] P. Manasa, C. K. Jayasankar, *Opt. Mater.* **2016**, *62*, 139.
[36] R. Vijayakumar, K. Maheshvaran, V. Sudarsan, K. Marimuthu, *J. Lumin.* **2014**, *154*, 160.
[37] R. Chakrabarti, M. das, B. Karmakar, K. Annapurna, S. Buddhudu, *J. Non-Cryst. Solids* **2007**, *353*, 1422.
[38] M. Gokce, *J. Non-Cryst. Solids* **2019**, *505*, 272.
[39] D. L. A. Dexter, *J. Chem. Phys.* **1953**, *21*(5), 836.
[40] H. Duan, R. Cui, X. Qi, C. Deng, *J. Mol. Struct.* **2020**, *1205*, 127551.
[41] X. Geng, Y. Xie, Y. Y. Ma, Y. Y. Liu, J. M. Luo, J. X. Wang, R. J. Yu, B. Deng, W. M. Zhou, *J. Alloys Compd.* **2020**, *847*, 156249.
[42] F. Jiang, S. Sha, S. Li, S. Xu, H. Xu, X. Mei, Y. Zhang, *Ceram. Int.* **2021**, *47*, 13776.

[43] M. Vijayakumar, P. Jayanthi, K. Marimuthu, *Opt. Mater.* **2019**, *93*, 44.
[44] A. Maity, S. Jana, S. Mitra, *Mater. Res. Bull.* **2022**, *146*, 111595.
[45] R. W. Liu, M. J. Chen, X. R. Zhu, Y. Y. Zhou, F. M. Zeng, Z. M. Su, *J. Lumin.* **2020**, *226*, 117378.
[46] P. Li, M. Peng, X. Yin, Z. Ma, G. Dong, Q. Zhang, J. Qiu, *Opt. Express* **2013**, *21*, 18943.
[47] M. K. Sahu, J. Mula, *J. Am. Ceram. Soc.* **2019**, *102*, 6087.
[48] G. Hirokazu Masaia, T. I. F. Okadab, N. Kawaguchid, *J. Lumin.* **2019**, *207*, 316.

How to cite this article: P. R. Babu, D. Gelija, K. S. Pasupuleti, B. K. Kumar, N. J. Sushma, M.-D. Kim, B. D. P. Raju, *Luminescence* **2023**, *38*(1), 71. https://doi.org/10.1002/bio.4422